A Pendulous Oscillating Gyroscopic Accelerometer Fabricated Using Deep-Reactive Ion Etching

Todd J. Kaiser, *Member, IEEE,* and Mark G. Allen, *Member, IEEE*

***Abstract*—A silicon pendulous oscillating gyroscopic accelerometer (POGA) was fabricated using deep-reactive ion etching (DRIE) and silicon wafer bonding technologies. A POGA is the micromachining-compatible analog of the pendulous integrating gyroscopic accelerometer (PIGA), which is the basis of the most sensitive accelerometers demonstrated to date. Gyroscopic accelerometers rely on the principle of rebalancing an acceleration-sensing pendulous mass by means of an induced gyroscopic torque. The accelerometer is composed of three individual layers that are assembled into the final instrument. The top layer uses wafer bonding of an oxidized wafer to a handling wafer to create a silicon-on-oxide wafer pair, in which the oxide layer provides electrical isolation between the mechanical members and the handling layer. The middle layer is a two-gimbal torsionally-supported silicon structure and is in turn supported by an underlying drive/sense layer. The micromachined POGA operated according to gyroscopic accelerometer principles, having better than milligram resolution and dynamic ranges in excess of 1 g (open loop) and approximately 12 mg (closed loop). [888]**

***Index Terms*—Accelerometer, deep-reactive ion etching (DRIE), inertial instruments, wafer bonding.**

I. Introduction

THE pendulous oscillating gyroscopic accelerometer (POGA) is the oscillatory analog of the pendulous integrating gyro accelerometer (PIGA), the most accurate strategic-grade accelerometer to date [1]. Instead of rotating members as in the PIGA, the members of the three orthogonal axis system in the POGA oscillate [2]. The interaction of the oscillations of the inner and outer members provides a dc torque to the middle member to rebalance a pendulous seismic mass. Because the members oscillate rather than rotate, significant design and manufacturing simplifications are possible. The oscillatory nature of the POGA makes it amenable to layered fabrication, which is achievable using micromachining technologies [3]. The operation of the POGA is easiest understood if the operation of the PIGA is first reviewed. The PIGA is the superposition of two instruments, a pendulous accelerometer and a single-degree-of-freedom gyroscope. The accelerometer is used to sense the accelerations and the gyroscope is used to maintain the proof mass at the null position through closed-loop operation.

Manuscript received June 17, 2002; revised August 29, 2002. Subject Editor E. Obermeier.

T. J. Kaiser was with the School of Electrical and Computer Engineering, Georgia Institute of Technology, Atlanta, GA 30332-0269 USA. He is now with the Department of Electrical and Computer Engineering, Montana State University, Bozeman, MT 59717-3780 USA (e-mail: tjkaiser@ece.montana.edu).

M. G. Allen is with the School of Electrical and Computer Engineering, Georgia Institute of Technology, Atlanta, GA 30332-0269 USA.

Digital Object Identifier 10.1109/JMEMS.2002.807476

Adding a proof mass to a symmetric gimbal can form a pendulous accelerometer (see Fig. 1). An input acceleration will create a torque on the gimbal proportional to the mass (m), the displacement of the mass from the axis of rotation or moment arm (l) and the input acceleration (a). This torque is defined as the *pendulous torque* τ_p:

$$\tau_p = mla. \tag{1}$$

Mounting a spinning momentum wheel on a gimbal perpendicular to the wheel axis forms a single-degree-of-freedom gyroscope. Rotation of the gyroscope about an axis perpendicular to both the spin axis of the wheel and the gimbal axis will create a *gyroscopic torque* τ_g on the gimbal proportional to the angular momentum of the wheel (H) and the rotation rate of the gyroscope (Ω) [4]–[6]:

$$\tau_g = H\Omega. \tag{2}$$

When the functionalities of the two instruments are superimposed, the gimbal of the accelerometer and the gimbal of the single-degree-of-freedom gyroscope become the same member. The pendulous torque and the gyroscopic torque are mechanically summed on this member, which is known as the *torque summing member* (TSM). The momentum wheel or rotor is usually positioned such that the spin axis is aligned with the pendulous mass as in Fig. 1. In order to generate a gyroscopic torque to balance the torque generated by the acceleration of the pendulous mass, the gyroscope is mounted on an additional member that is able to rotate under the influence of an external servomotor. This member is called the *servo driven member* (SDM). In closed-loop operation of the PIGA, the SDM is rotated such that the gyroscopic and pendulous torques cancel. Setting the pendulous torque equal to the gyroscopic torque creates an equilibrium torque equation given by

$$mla = I_1\dot{\psi}\dot{\phi} \tag{3}$$

where I_1 is the moment of inertia of the rotor about the spin axis, $\dot{\psi}$ is the angular velocity of the rotor about the spin axis and $\dot{\phi}$ is the angular velocity of the servo driven member about its axis.

In order to null a constant input acceleration, such as the acceleration due to Earth's gravity, a constant rotation of the SDM is required, which is a potential disadvantage of the PIGA approach. The electrical signals must pass through sliprings to excite the inner components. These sliprings can eventually become failure modes, due to the wear caused by the continuous rotation of the SDM.

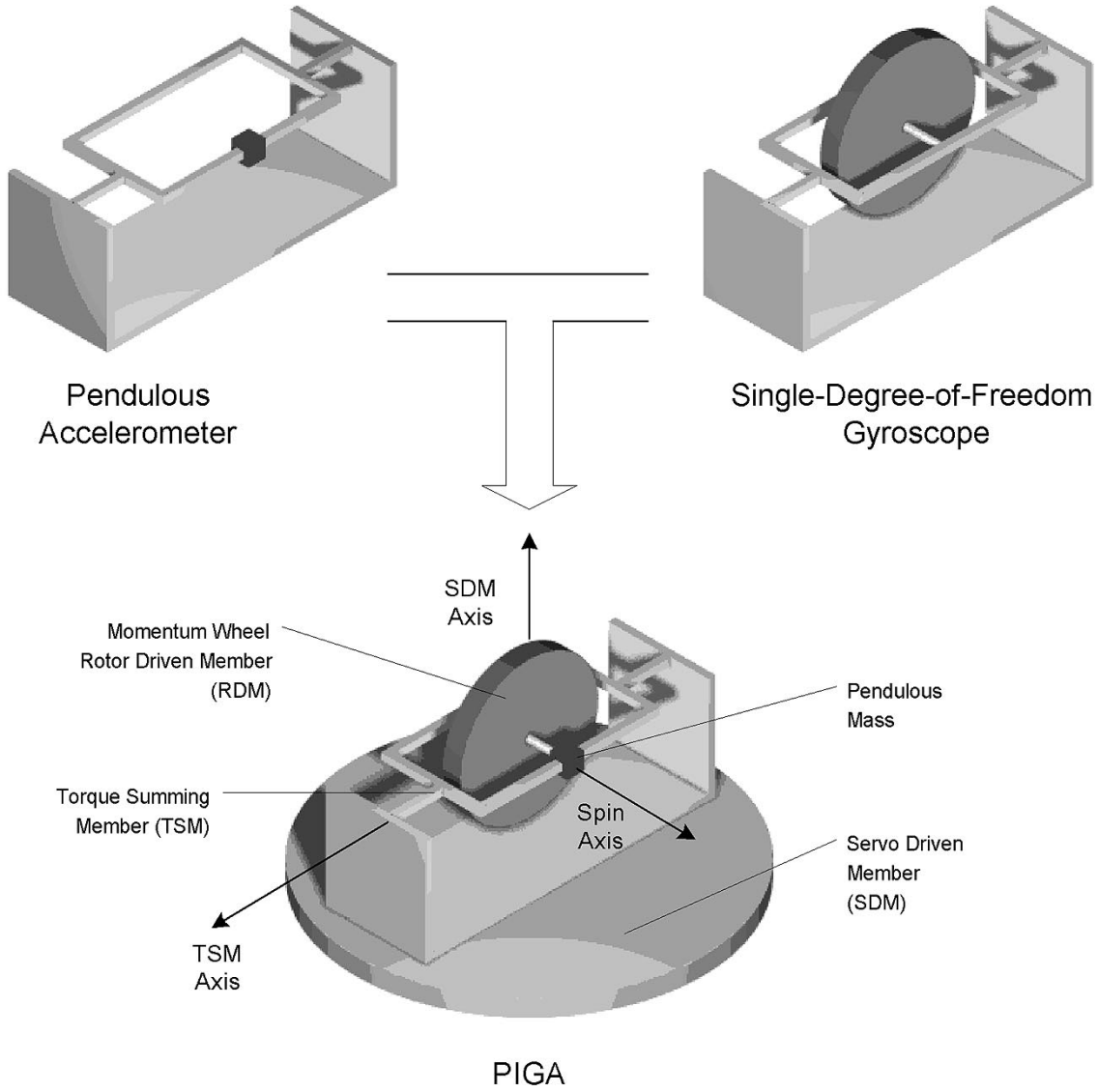

Fig. 1. The PIGA is the combination of a pendulous accelerometer and a single-degree-of-freedom gyroscope.

The replacement of the rotating members with oscillating members is the fundamental design change between the PIGA and POGA. It eliminates the vulnerable sliprings and makes the device suitable for microfabrication, while maintaining the fundamental physics that has produced the highest performing accelerometers.

The POGA is also a three orthogonal axis system. Instead of rotating members as in the PIGA, the members are supported by flexures as in Figs. 2 and 3 and designed to oscillate. The inner member, designated the rotor-driven member (RDM), generates the angular momentum just as in the PIGA, but instead of a fixed angular momentum, the angular momentum oscillates. The oscillating angular momentum requires an oscillating SDM to generate the gyroscopic torque that nulls the TSM. If the RDM and SDM are forced to oscillate at the same frequency ω, then the equilibrium torque equation can be given by

$$mla = I_1\dot{\psi}\dot{\phi} = I_1\Psi\Phi\omega^2\sin(\omega t)\sin(\omega t+\beta) \qquad (4)$$

where Ψ and Γ are the amplitude of oscillation of the RDM and SDM and β is phase difference between their oscillations. Trigonometric and algebraic manipulations produce the resulting expression for the acceleration:

$$a = \frac{I_1\Psi\Phi}{2ml}\omega^2\cos\beta + f(2\omega). \qquad (5)$$

The acceleration is a function of the cosine of the phase difference between the two oscillations plus a second harmonic term that time averages to zero. The phase difference becomes the control signal used to maintain the TSM at null in a closed-loop POGA.

II. Device Design

Fig. 3 shows a schematic of the micromachined POGA. The angular momentum is generated by the RDM about the spin axis. The TSM torques about the input axis with an input acceleration along the output axis. Several design restrictions were implemented in the layout of the micromachined POGA. The

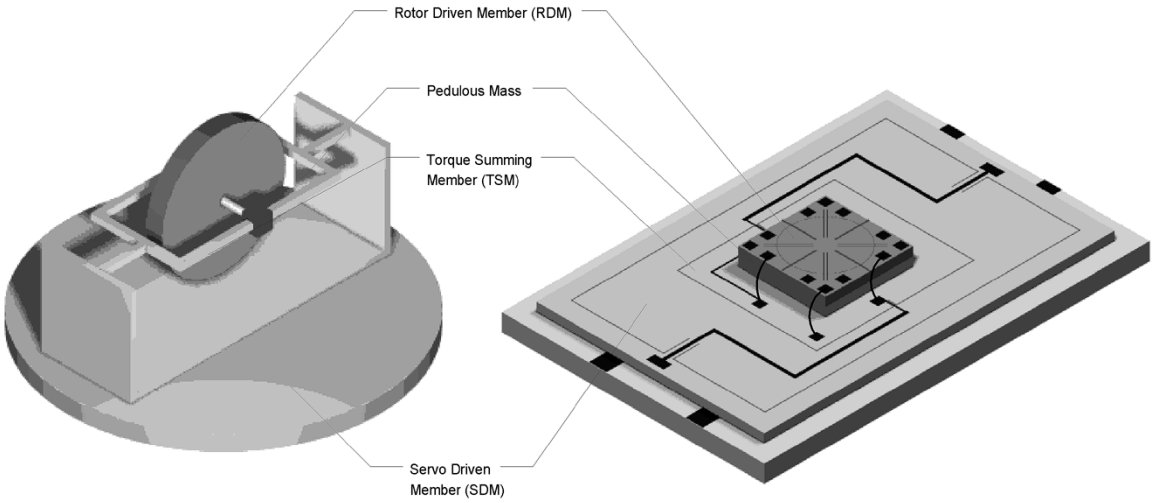

Fig. 2. The POGA is the oscillatory analog of the PIGA. The pendulous mass in the micromachined POGA is the RDM layer since it is out of the plane of the TSM.

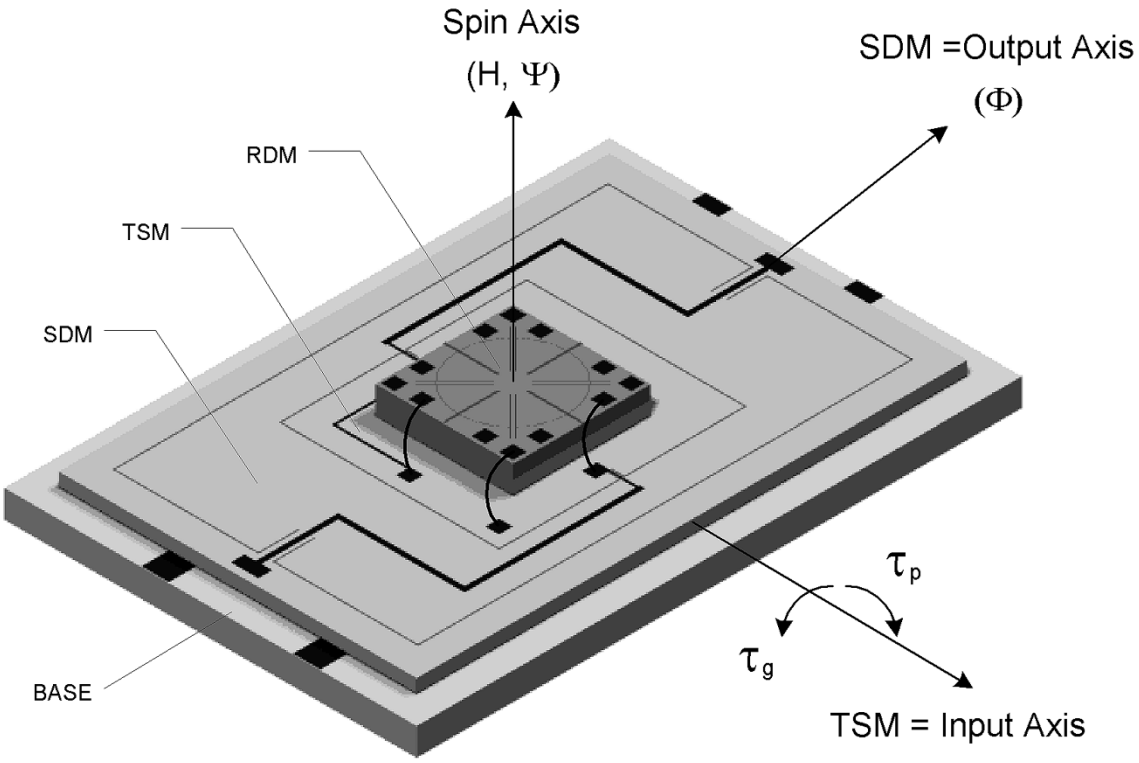

Fig. 3. Schematic drawing of the micromachined POGA showing the principal components and rotational axes.

first restriction was a product of the manufacture method and the fabrication material. Silicon was chosen for the base material for its excellent mechanical properties [7] and for its capability to be deep reactive ion etched [8]. Another design restriction focused on the actuation method. It was desired to actuate the driven members electrostatically under ambient pressure. The choice of an electrostatic drive stems from the ease of fabrication of this type of actuator, while the ambient pressure restriction eliminates the necessity of vacuum packaging.

Since the nature of the POGA leads to the desire to maximize the angular momentum generated by the motion of the RDM, a design criterion is to maximize the physical size of the RDM subject to the constraints of electrostatic drive and microfabrication. The RDM of the micromachined POGA is a 4.5-mm diameter silicon member formed by etching entirely through a 300-μm-thick 2-in wafer. It has two sets of four rotational electrostatic comb drives for in-plane actuation. The RDM is supported by four 50 μm-wide silicon flexures that are anchored to an underlying layer of silicon. The spacing between the comb fingers is 50 μm. The comb drives and anchors are electrically isolated from each other by thermally grown silicon dioxide. An actuation voltage of 90 V created a $\pm 0.5^{\circ}$ oscillation at resonance frequencies ranging from 1300 to 2200 Hz with a quality factor of approximately 100.

The TSM and the SDM are silicon members etched from the same two-inch silicon wafer as a single unit. The TSM is inset within the SDM. The TSM flexures are 50 μm wide and 1 mm long connecting the TSM to the SDM. The SDM flexure dimensions are varied to match the SDM resonant frequency to the RDM resonant frequency. These flexures attach the SDM to a frame that is mounted to a supporting base. The SDM has 100 μm holes perforating the silicon structure to reduce the squeeze film damping between the SDM and the supporting glass base. The TSM requires damping to reduce the vibration sensitivity of the TSM, so no perforations are necessary. The backside of the SDM and TSM are etched to create the necessary gap to allow motion of these members. This gap was varied between 10 and 50 μm. Smaller gaps required less drive voltages but allow smaller mechanical motion. The front side has electrical conduits patterned on the surface separated from the substrate by a layer of silicon dioxide.

The SDM/TSM assembly is mounted on a base that provides electrodes for actuation and sensing of the mechanical members. The drive electrodes for the SDM are positioned near the edge of the member to increase the torque generated. The SDM sensing electrodes are positioned just inside the drive electrodes. The TSM 2 mm $\times$ 5 mm sensing electrodes are placed under the TSM at the edge of the member to maximize sensitivity to rotations. They have a 50-μm gap that results in a 2 pf capacitance. Both sensor systems use differential capacitor readout electronics to monitor the position of the SDM and TSM. A ground plane is serpentined between the electrodes to reduce crosstalk between the capacitors.

III. Fabrication

The micromachined POGA is fabricated in three separate assemblies, the RDM, the SDM/TSM assembly and the base. The RDM and SDM/TSM assembly were etched out of silicon wafers in a Plasma Therm inductively coupled plasma reactive ion etcher (ICP-RIE). Characterization and discussion of the procedure can be found elsewhere [8]. The base is formed in glass with patterned metal electrodes on the surface.

The RDM fabrication sequence is shown in Fig. 4. A 2-in p-type silicon wafer is oxidized to produce a 1 μm layer of oxide surrounding the wafer. The oxidized wafer is bonded to another nonoxidized wafer using standard techniques [9]. The bonded wafers are now electrically isolated by the oxide layer between them. The bonded wafers are then oxidized again. The top wafer is then patterned and etched down to the buried oxide layer defining the RDM, its flexures and its radial comb drives. The wafer combination is then etched from the backside to release the RDM mechanical structure, yet retain the anchors for the flexures and comb drive. The oxide is then removed from the exterior surfaces and aluminum is patterned on the comb drive anchors by using a shadow mask.

The shadow masks were also produced using the ICP. Holes were etched through silicon wafers to produce the masks. When the mask is aligned to the wafer, aluminum was allowed to deposit on the component only in the required areas. The shadow masks were produced for both device-level metallization and wafer-level metallization.

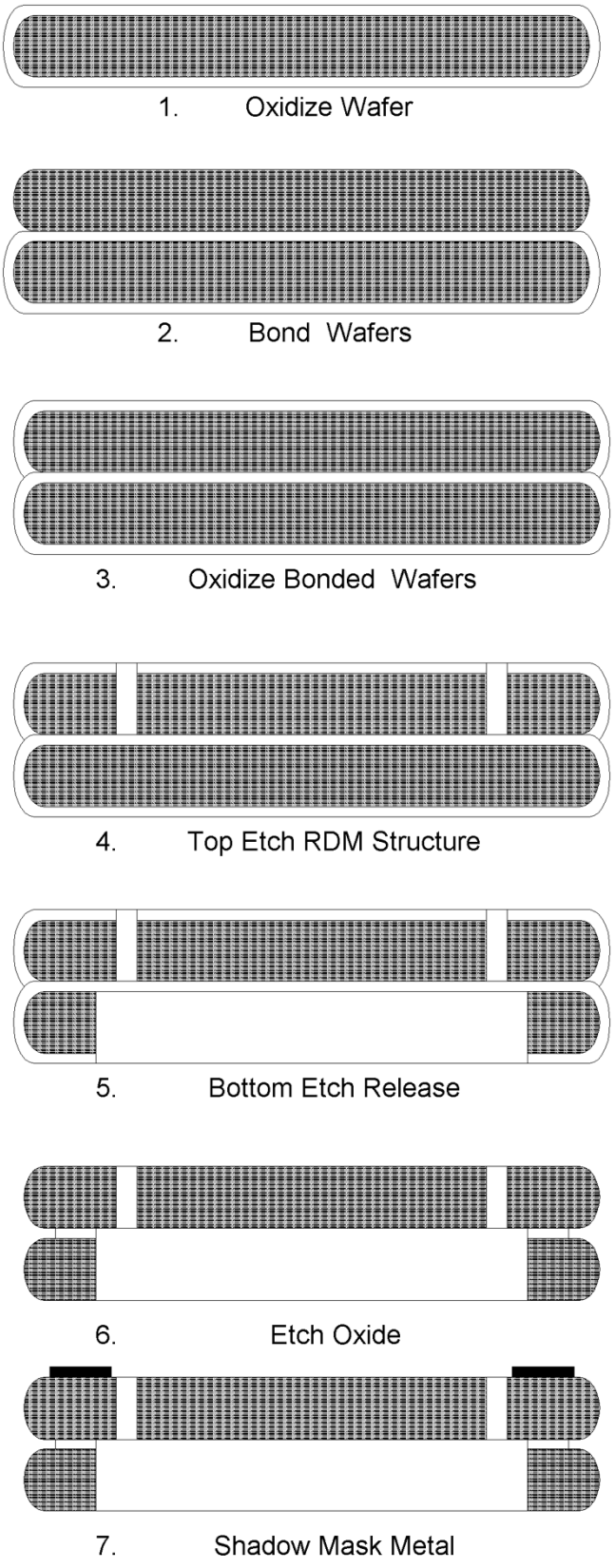

Fig. 4. RDM fabrication sequence.

The fabrication sequence of the SDM/TSM assembly is shown in Fig. 5. A p-type 2-in silicon wafer is oxidized to produce a one micron layer of oxide. Windows are etched in

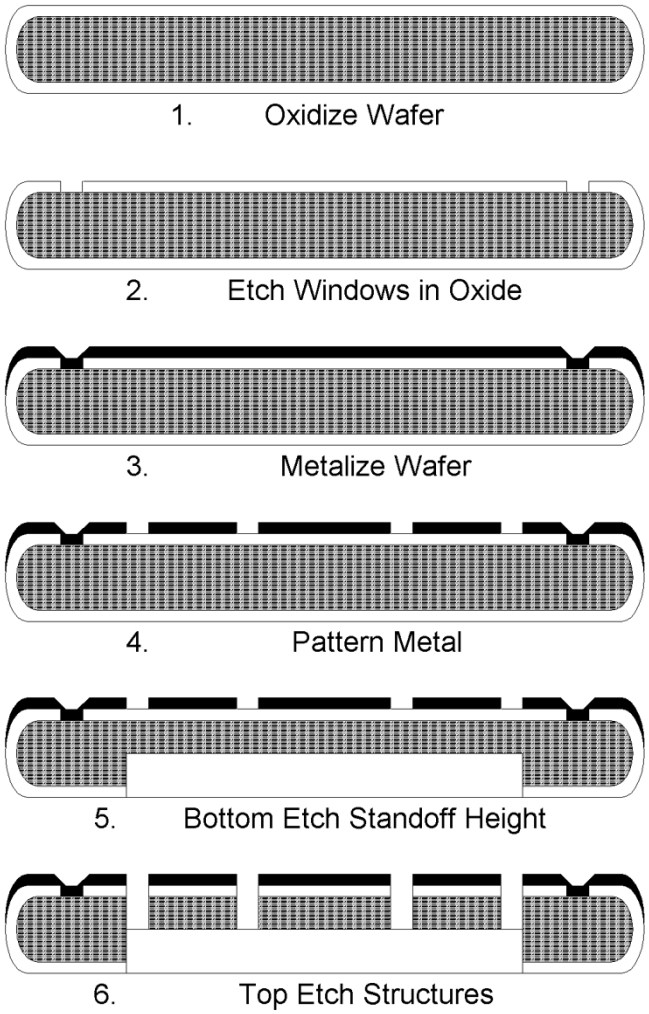

Fig. 5. SDM/TSM assembly fabrication sequence.

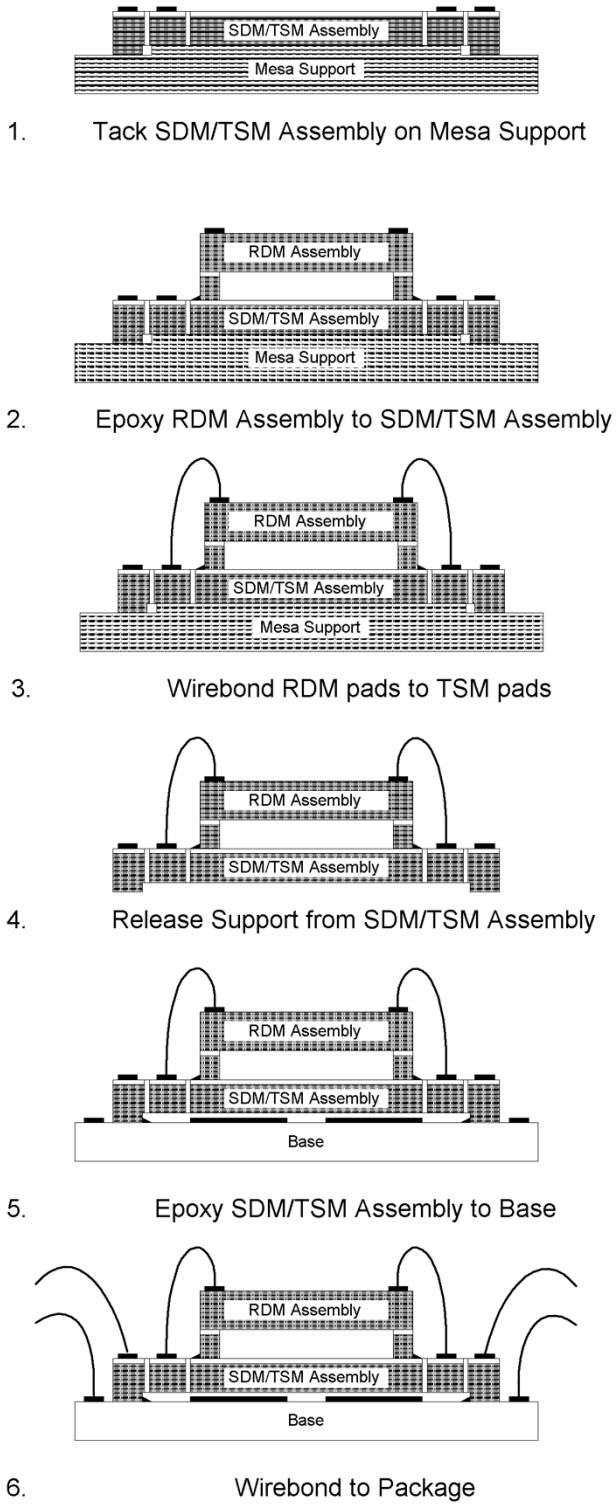

Fig. 6. Micromachined POGA assembly procedure.

the oxide to provide contact regions to the silicon. Aluminum is deposited on the wafer, sintered then patterned. The backside of the wafer is etched to produce the standoff height between the base metal layers and the silicon mechanical layers. The wafer is then etched entirely through its thickness from the front side to define the SDM and TSM.

The bases are formed in glass. Aluminum is deposited on the glass with a titanium adhesion layer. The metals are then patterned to produce the SDM drive electrodes and the sensing electrodes for the SDM and TSM.

The three components are then assembled to form the instrument. The assembly procedure is shown in Fig. 6. The SDM/TSM assembly is temporarily mounted on a mesa support structure. The mesa is used to handle the component and support the movable members during assembly. The RDM is positioned on the TSM and epoxied in place. A recess in the TSM aids in the alignment of the RDM to the TSM. Electrical connections are made from the RDM by wirebonding. The SDM/TSM assembly is released from the supporting mesa and epoxied to the glass base. The base is then wirebonded to the package.

Fig. 7 shows an RDM still in a device array on the wafer. Small tabs are left during the etching process to interconnect the components. These are easily cleaved to dice out the individual components. Fig. 8 is an SDM/TSM assembly. The SDM axis of rotation is horizontal in the image with electrical connections running to the perimeter. The TSM axis of rotation is vertical in the image with the electrical conduit running across the surface of the flexures. Fig. 9 shows a base with the electrode layout visible. The SDM requires both sensing and drive capac-

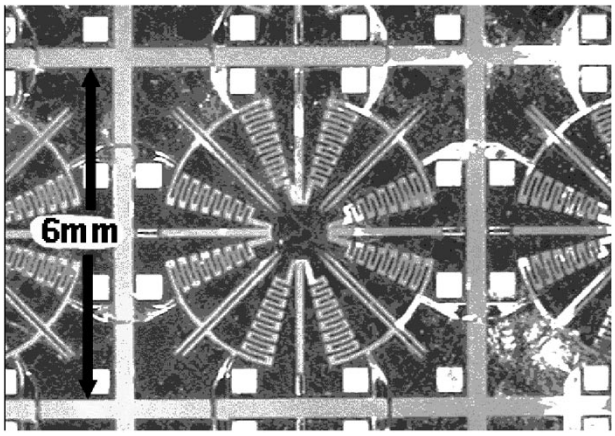

Fig. 7. is an image of a single RDM in an array of devices. Each RDM has a diameter of 4.5 mm formed in a 6 × 6 mm silicon die connected by tabs.

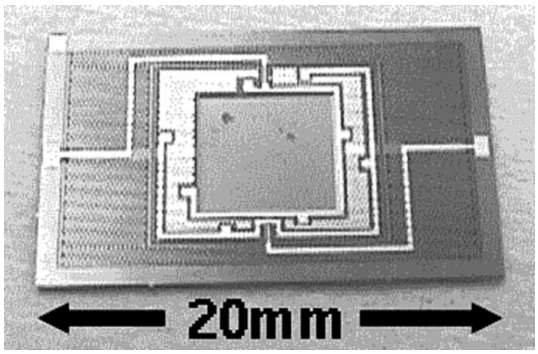

Fig. 8. is an image of an SDM/TSM assembly with a recess for mounting the RDM on the TSM. Aluminum conduits isolated by an oxide layer run along the surface. The SDM frame measures 13 × 20 mm.

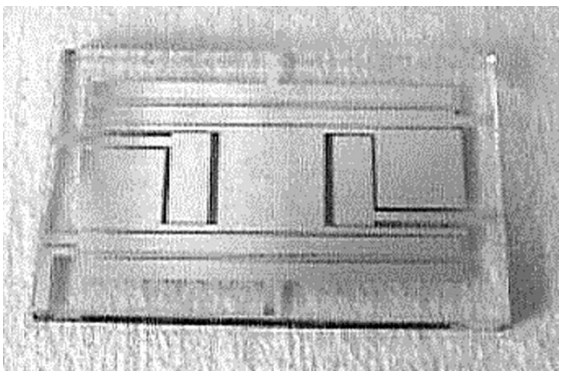

Fig. 9. The glass bass of the micromachined POGA, 15 × 22 mm.

itive electrodes while the TSM requires only a pair of sensing electrodes. Fig. 10 shows the assembled micromachined POGA. Fig. 11 is a scanning electron microscope (SEM) image of the RDM and SDM. The RDM flexure runs vertically in the image between the radial comb drives. A wire bond from the comb drive is visible on the right side of the image. The edges of the two bonded layers of the RDM and the perforations in the SDM/TSM layer are visible.

IV. Testing

Open loop, the POGA operates just like any other pendulous accelerometer. Under acceleration, the pendulous mass torques

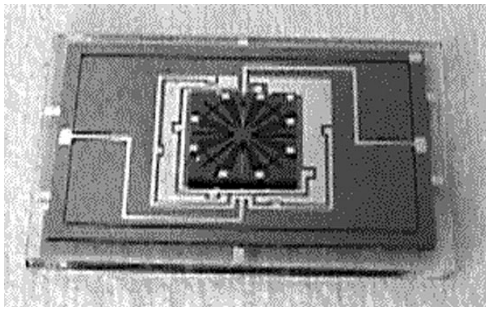

Fig. 10. Image of an assembled micromachined POGA. The RDM mounts on the TSM and the SDM/TSM assembly mounts on the base.

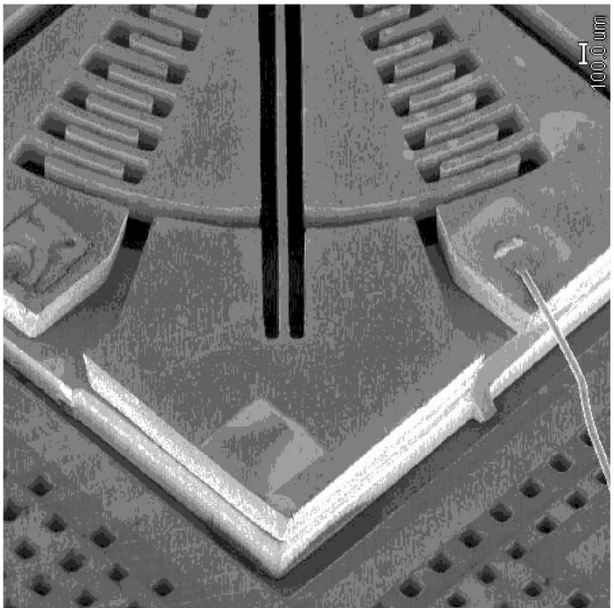

Fig. 11. SEM of a quadrant of the RDM.

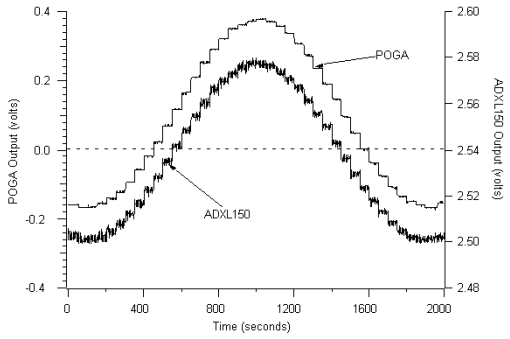

Fig. 12. Open loop tumble test of ADXL150 and micromachined POGA. Rotated 10° steps at 50-s intervals measuring a component of earth's gravity.

the TSM against the supporting flexures. The TSM motion is detected through the differential plate capacitors connected through current transformers to custom readout electronics. Fig. 12 shows an open loop tumble test of the bulk micromachined POGA and an ADXL150, an Analog Devices 50 g micromachined accelerometer. The instruments are mounted on a dividing head and rotated at 10° steps through 360°, measuring the component of the earth's gravity along the input axis of the accelerometers.

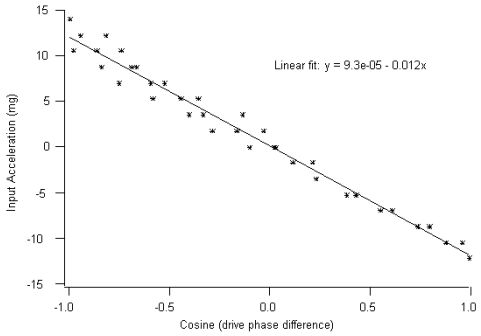

Fig. 13. Closed loop scale factor test. Input acceleration nulled by adjusting phase between input drive voltages.

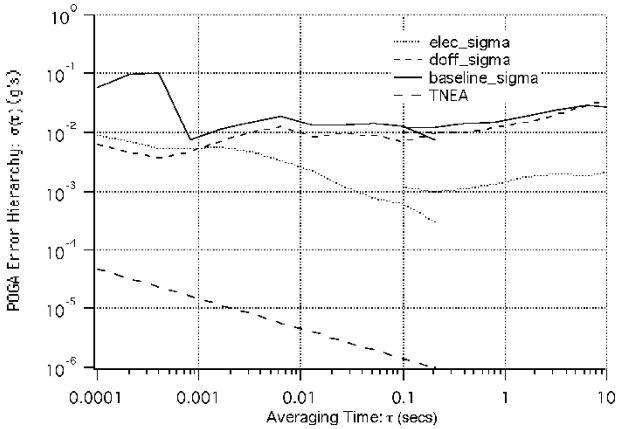

Fig. 14. Allan deviation of the electronics, the open loop pendulous accelerometer, the baseline POGA and the thermal noise equivalent acceleration.

Closed loop, the POGA operation differs from other accelerometers. The innermost member, the RDM, generates an oscillating angular momentum. The drive frequency is set at the resonant frequency of the RDM. A bias voltage is applied to the sinusoidal signal to offset the drive so that it is always applying a positive potential to remove the frequency doubling effect of capacitive electrostatic actuators. The oscillating angular momentum is the functional equivalent to the constant angular momentum of a spinning wheel gyro. In the PIGA, the pendulous mass is torqued back to the null position by spinning the SDM to generate the gyroscopic torque. Similarly, the SDM of the POGA oscillates to create a torque that nulls the TSM. The drive voltage of the SDM is phase locked to the RDM drive. A bias voltage is also applied to remove frequency-doubling effects. By controlling the relative phase and magnitude of the RDM and SDM oscillations, the central pendulous torque summing member can be held at null.

Fig. 13 shows the results of the closed-loop scale factor test. The POGA was positioned such that the input axis of the accelerometer was vertical on a dividing head. The dividing head was then rotated to produce an input acceleration. The input acceleration was sensed by the TSM causing a shift in the output voltage. Keeping the RDM and SDM drive magnitudes constant, the TSM position voltage was then returned to the null position by manually adjusting the phase difference between the phase locked function generators used to drive the RDM and SDM. The input acceleration was calculated by taking the sine of the angle on the dividing head. Equation (5) shows the input acceleration should be a linear function of the cosine of the phase, experimentally confirmed in Fig. 13.

The stability of the accelerometer data was analyzed using the methods developed by Allan for atomic clocks [10] and adapted for inertial measurement instruments [11], [12]. The Allan variance and deviation of the data when calculated and plotted against increasing integration times creates plots that reveal signature noise characteristics of the data. White noise will have a $-1/2$ slope, $1/f$ noise will have a zero slope and random walk and drift will have $+1/2$ slope in a log-log plot of Allan deviation versus integration time.

The fundamental limit of this instrument is the thermal noise created by the impinging of atoms on the mechanical members. The magnitude of the thermal-mechanical noise depends on the temperature and damping of a spring-mass system. The thermal noise equivalent acceleration (TNEA) is given by (6) [13].

$$\text{TNEA} = \sqrt{\frac{4kT\omega_0}{IQ}}\left(\frac{g}{\sqrt{Hz}}\right) \tag{6}$$

where k is the Boltzman constant, T is the temperature, ω_0 is the resonant frequency of the TSM, I is the moment of inertia of the TSM and Q is the mechanical quality factor. An estimate of the fundamental limit of the micromachined POGA was obtained by inserting the necessary parameters into (6). A value of was calculated. A white noise Allan deviation was calculated by substituting the thermal-mechanical noise term into the expression [10]–[12]:

$$\sigma_0 = \sqrt{\frac{h_0}{2\tau}} \tag{7}$$

where σ_0 is a white noise Allan deviation term, h_0 is the TNEA squared and τ is the integration time of the Allan deviation. The thermal noise equivalent acceleration was plotted in Fig. 14. Additional Allan deviations were calculated for three additional conditions. This created a hierarchy of error sources that contributed to the ultimate stability of the instrument. The electronic readout system noise characteristics were measured by replacing the variable capacitors of the instrument with fixed capacitors. This gave a measurement of the contribution of the electronics to the total noise characteristic (elec_sigma in Fig. 14). A measurement of the noise of the pendulous accelerometer was taken by monitoring the TSM output without activating the drives of the RDM and SDM (doff_sigma). The final Allan deviation was the baseline configuration of the POGA. Both the RDM and SDM were actuated at the operational frequency of 1174 Hz. This frequency coupled into the output measurement of the torque summing member. This is seen Fig. 14 by the large hump between 1 ms and 100 μs. The motion of the SDM was coupling into the sensor of the TSM. This could be significantly reduced if the capacitor sensors for the TSM were moved from the underlying base to the SDM itself. In this configuration the sensor would move with the SDM and would then be only sensitive to motion of the TSM. The discontinuities seen in Fig. 14 are the results of

repeating the measurement for long integration times. This was necessary due to the limits of the data acquisition system.

V. Conclusion

The POGA uses the same fundamental physics that has been demonstrated to produce the highest performing accelerometer, the PIGA. The scale factor is determined by mechanical quantities, the pendulosity and angular momentum rather than precision reference signals as in other servoed accelerometers. In the design application specific layers were produced then assembled into an instrument. The stacked layer design in conjunction with bulk micromachjning is ideally suited for modern inertial sensors where reduced cost and high performance are required.

Acknowledgment

The authors would like to acknowledge the Special Projects Office of the US Navy, SP-23, who funded the early effort to demonstrate the POGA proof-of-principle model with conventional construction and subsequently motivated the demonstration of the silicon micromachined POGA. Microfabrication was carried out in the Georgia Tech Microelectronics Research Center. They would also like to thank the staff of Milli Sensor Systems and Actuators for their numerous contributions as well as their discussions of capacitive sensing.

References

[1] M. S. Sapuppo, "Pendulous oscillating gyro accelerometer: POGA," *Joint Services Data Exchange for Guidance, Navigation & Control, 24th*, Nov. 1998.

[2] ——, "Pendulous Oscillating Gyro Accelerometer," U.S. Patent #5 457 993, Oct. 17, 1997.

[3] T. J. Kaiser and M. G. Allen, "A micromachined pendulous oscillating gyroscopic accelerometer," in *Tech. Dig. 2000 Solid State Sensor and Actuator Workshop*, Hilton Head, SC, 2000, pp. 85–88.

[4] A. Lawrence, *Modern Inertial Technology*. New York: Springer-Verlag, 1998.

[5] G. R. Pitman, *Inertial Guidance*, G. R. Pitman, Ed. New York: Wiley, 1962.

[6] M. Fernandez and G. R. Macomber, *Inertial Guidance Engineering*. Englewood Cliffs, NJ: Prentice-Hall, 1962.

[7] K. E. Petersen, "Silicon as a mechanical material," *Proc. IEEE*, vol. 70, no. 5, pp. 420–457, 1982.

[8] A. A. Ayon, R. Braff, C. C. Lin, H. H. Sawin, and M. A. Schmidt, "Characterization of a time multiplexed inductively coupled plasma etcher," *J. Electrochem. Soc.*, vol. 146, no. 1, pp. 339–349, 1999.

[9] M. A. Schmidt, "Silicon wafer bonding for micromechanical devices," in *Tech. Dig. 1994 Solid State Sensor and Actuator Workshop*, Hilton Head, SC, 1994, pp. 127–131.

[10] D. W. Allan, "Statistics of atomic frequency standards," *Proc. IEEE*, vol. 54, no. 2, pp. 221–230, Feb. 1966.

[11] C. R. Kochakian, "Time-Domain uncertainty charts (Green Charts): A tool for validating the design of IMU/instrument interfaces," in Proceedings of the AIAA Guidance and Control Conference, August 11–13, 1980.

[12] G. W. Erickson, "An overview of dynamic and stochastic modeling of gyros," in *Proc. Inst. Navigation National Technical Meeting*, Jan. 20–22, 1993, pp. 339–351.

[13] T. B. Gabrielson, "Fundamental noise limits for miniature acoustic and vibration sensors," *J. Vibration Acoust.*, vol. 117, no. 4, pp. 405–410, Oct. 1995.

Todd J. Kaiser (M'00) received the B.S. degree in physics from Montana State University, Bozeman, in 1981, the M.S. degree in physics from Oregon State University, Corvallis, in 1984, and the Ph.D. degree in electrical engineering from Georgia Institute of Technology, Atlanta, in 2000.

He designed optical gyroscopes at Draper Laboratory, Cambridge, MA, from 1985 to 1994. From 1994 to 2000, he was a program manager for the development of micromechanical inertial instruments at Milli Sensor Systems and Actuators (MSSA). Currently, he is an Assistant Professor at Montana State University, Bozeman. His research interests include MEMS fabrication, inertial sensors and micromechanical actuators and sensors.

Mark G. Allen (M'89) received the B.A. degree in chemistry, the B.S.E. degree in chemical engineering, and the B.S.E. degree in electrical engineering from the University of Pennsylvania, University Park, and the S.M. and Ph.D. degrees from the Massachusetts Institute of Technology, Cambridge, in 1989.

He joined the faculty of the Georgia Institute of Technology, Atlanta, in 1989, where he currently holds the rank of Professor and the J. M. Pettit Professorship in Microelectronics. His research interests are in the areas of micromachining and microelectromechanical systems (MEMS); in particular, the development and application of new fabrication technologies for micromachined devices and systems. He was General Co-Chair of the 1996 IEEE MEMS conference and is North American editor of the *Journal of Micromechanics and Microengineering.*